Adsorption of supercritical CO_2 in aerogels as studied by small-angle neutron scattering and neutron transmission techniques

Y. B. Melnichenko[a] and G. D. Wignall
Condensed Matter Sciences Division, Oak Ridge National Laboratory, Oak Ridge, Tennessee 37831-6393

D. R. Cole
Chemical Sciences Division, Oak Ridge National Laboratory, Oak Ridge, Tennessee 37831-6110

H. Frielinghaus
Forschunszentrum Jülich, Institut für Festkörperforschung, D-52425 Jülich, Germany

(Received 8 August 2005; accepted 11 April 2006; published online 26 May 2006)

Small-angle neutron scattering (SANS) has been used to study the adsorption behavior of supercritical carbon dioxide (CO_2) in porous Vycor glass and silica aerogels. Measurements were performed along two isotherms ($T=35$ and 80 °C) as a function of pressure (P) ranging from atmospheric up to 25 MPa, which corresponds to the bulk fluid densities ranging from $\rho_{CO_2} \sim 0$ to 0.9 g/cm^3. The intensity of scattering from CO_2-saturated Vycor porous glass can be described by a two-phase model which suggests that CO_2 does not adsorb on the pore walls and fills the pore space uniformly. In CO_2-saturated aerogels an adsorbed phase is formed with a density substantially higher that of the bulk fluid, and neutron transmission data were used to monitor the excess adsorption at different pressures. The results indicate that adsorption of CO_2 is significantly stronger in aerogels than in activated carbons, zeolites, and xerogels due to the extremely high porosity and optimum pore size of these materials. SANS data revealed the existence of a compressed adsorbed phase with the average density ~ 1.07 g/cm^3, close to the density corresponding to closely packed van der Waals volume of CO_2. A three-phase model [W. L. Wu, Polymer **23**, 1907 (1982)] was used to estimate the volume fraction ϕ_3 of the adsorbed phase as a function of the fluid density, and gave $\phi_3 \sim 0.78$ in the maximum adsorption regime around $\rho_{CO_2} \sim 0.374$ g/cm^3. The results presented in this work demonstrate the utility of SANS combined with the transmission measurements to study the adsorption of supercritical fluids in porous materials. © *2006 American Institute of Physics*. [DOI: 10.1063/1.2202324]

I. INTRODUCTION

A supercritical fluid (SCF) is a substance at a pressure and temperature above its liquid-gas critical point where the coexisting (subcritical) liquid and gaseous phases become indistinguishable. At high pressure, the density of an SCF may become sufficient to provide substantial solvent power. At the same time, the diffusivity of solutes in SCFs is higher than in liquids due to a much lower viscosity, which facilitates mass transfer. The combination of tunable solvent power, practically unlimited miscibility with gases as well as advantageous mass transfer properties make SCFs an attractive alternative to subcritical (liquid) solvents for a variety of technological applications such as heterogeneous catalysis, adsorptive separations, regeneration of adsorbers, and SCF chromatography.[1] Simplified theoretical considerations of heterogeneous processes are often based on an assumption that supercritical solvents in porous media can be treated as a continuum and thus the adsorption of the solvent molecules by the surface of solid porous adsorbents can be ignored.[2] It is now being recognized, however, that when an adsorbate gas or supercritical fluid is in contact with a solid adsorbent, the attractive molecule-solid forces enhanced by strong micropore field effects can create a region near the solid surface where the local adsorbate density is different from that in the homogeneous bulk phase.[3,4] The adsorbed phase region is believed to extend to a distance of few molecular diameters from the surface far away from the critical point, and to become long ranged as the critical point is approached.[5] An understanding of the structure and thermodynamic properties of the adsorbed phase at different conditions is fundamental to the successful development and optimization of reaction and separation processes involving SCF-solid interactions.[6]

In this article we report the results of small-angle neutron scattering (SANS) and neutron transmission measurements of the adsorption of supercritical carbon dioxide (SC CO_2) on a nanoporous silica aerogel. We demonstrate that the neutron transmission data can provide information on the excess adsorption, which has traditionally been measured by gravimetric, volumetric, total desorption, and other methods. In turn, SANS can give complementary information on the density of the adsorbed phase and may be used to determine the volume fraction of this phase under certain conditions. The results demonstrate that high-pressure adsorption of CO_2 in aerogels is much stronger than in other porous materials commonly used in a variety of heterogeneous processes, due to the particular structure of these highly porous materials.

[a]Electronic mail: yui@ornl.gov

 © 2006 American Institute of Physics

Downloaded 21 Dec 2006 to 134.94.122.39. Redistribution subject to AIP license or copyright, see http://jcp.aip.org/jcp/copyright.jsp

We argue that SANS in conjunction with transmission measurements can be very effective characterization methods of the adsorption behavior of various single-component fluids and multicomponent-fluid mixtures in strongly adsorbing porous media of practical importance.

II. EXPERIMENTAL METHODS AND PROCEDURES

A. Excess and absolute adsorptions

Consider a system with the total volume V_{total} which consists of a solid adsorbent, unadsorbed fluid, and adsorbed phase with the volumes V_{solid}, V_{fluid}, and V_{ads}, respectively,

$$V_{\text{total}} = V_{\text{solid}} + V_{\text{fluid}} + V_{\text{ads}} = V_{\text{solid}} + V_{\text{void}}, \tag{1}$$

where V_{void} is the void volume accessible to the supercritical fluid. By definition, the *excess* adsorption (also known as the Gibbs adsorption) is the excess material present in the pores of the adsorbent over that corresponding to the density of the fluid in the bulk phase at the same temperature and pressure. Thus, in terms of the relative mass (n, g/g), the excess adsorption n_e can be represented as[7]

$$n_e = n_{\text{total}} - V_{\text{void}}\rho_{\text{fluid}}, \tag{2}$$

where n_{total} is the total amount (g/g) of supercritical fluid in the volume occupied by the adsorbent, V_{void} is the pore volume in cm^3/g, and ρ_{fluid} is the fluid density in g/cm^3. Equation (2) illustrates the physical meaning of the excess adsorption, which is calculated neglecting the volume occupied by the adsorbed phase, i.e., as if the entire void volume V_{void} was accessible to the unadsorbed (bulk) fluid.

Conversely, the *absolute* adsorption (n^{abs}) is calculated taking into account the reduction of the void volume accessible to the fluid due to formation of the adsorbed phase,

$$n^{\text{abs}} = n_{\text{total}} - V_{\text{fluid}}\rho_{\text{fluid}}. \tag{3}$$

Equations (2) and (3) can be rearranged to give

$$n_e = V_{\text{ads}}(\rho_{\text{ads}} - \rho_{\text{fluid}}), \tag{4}$$

and

$$n^{\text{abs}} = n_e\left(\frac{\rho_{\text{ads}}}{\rho_{\text{ads}} - \rho_{\text{fluid}}}\right). \tag{5}$$

Under supercritical conditions, the density of the fluid phase increases monotonically with pressure, whereas the density of adsorbed phase initially increases and then levels off at a value corresponding to the maximal amount of adsorbate which can be packed into the pores. Consequently, according to Eq. (4), the excess adsorption should initially increase, go through the maximum, become zero at $\rho_{\text{ads}}=\rho_{\text{fluid}}$, and finally become negative at higher pressures.[8] All conventional methods (gravimetric, volumetric, total desorption, isotope exchange, etc.) measure n_e as a function of temperature and pressure.[6] Equations (4) and (5) show that the calculation of the absolute adsorption from n_e requires information on the density of adsorbed phase, which is not readily accessible by existing experimental methods. The value of n^{abs} can be estimated based on a model and/or on equation of state calculations of ρ_{ads}.[9,10] Evidently, n^{abs} can be determined directly from experimental data in the limit $\rho_{\text{ads}} \gg \rho_{\text{fluid}}$ when $n^{\text{abs}} \cong n_e$ [see Eq. (5)]. It is important to note, however, that excess adsorption is the variable sufficient to describe the thermodynamics of the supercritical fluid adsorption and knowledge of n^{abs} is not absolutely necessary for technological calculations.[6]

B. Neutron transmission of multicomponent systems

The neutron transmission is a parameter measured in SANS experiments. It is one of the parameters used for converting the intensity of scattering in counts per second into a neutron cross section in units of cm^{-1}.[11] Here we demonstrate that neutron transmission data can provide information on the SCF adsorption at a variety of different conditions. The attenuation of a neutron beam passing through a porous adsorbent (e.g., silica aerogel) is due to scattering (coherent and incoherent) and absorption of neutrons by silicon and oxygen nuclei. The beam can be further attenuated if the aerogel contains adsorbing and or scattering impurities such as hydrogen containing alkyl groups (see discussion in Sec. III B). The transmission T_1 of a blank aerogel is described by Beer's law,[12]

$$T_1 \equiv \frac{I}{I_0} = T_0 \exp(-N_{\text{SiO}_2}\sigma_{\text{SiO}_2}t), \tag{6}$$

where I_0 and I are the incident and attenuated neutron intensities, respectively, N_{SiO_2} is the number of silica molecules per unit volume (number density of SiO_2), σ_{SiO_2} is the total neutron cross section of SiO_2, and t is the sample thickness. The prefactor $T_0 \leqslant 1$ accounts for the additional attenuation of the neutron beam due to impurities.

The saturation of an aerogel with a fluid (e.g., SC CO_2) should decrease the total transmission due to additional fluid density-dependent attenuation of the beam caused by scattering and absorption of neutrons by CO_2. The transmission of the two-phase system representing aerogel matrix (phase 1) homogeneously saturated with a nonadsorbing fluid (phase 2) is given by

$$\begin{aligned} T_2 &= \exp(-N_{\text{SiO}_2}\sigma_{\text{SiO}_2}t - N_{\text{CO}_2}\sigma_{\text{CO}_2}t) \\ &= T_1 \exp(-N_{\text{CO}_2}\sigma_{\text{CO}_2}t). \end{aligned} \tag{7}$$

The number density (N_{CO_2}) and physical density (ρ_{CO_2}) of CO_2 are related via

$$N_{\text{CO}_2} = \rho_{\text{CO}_2}\frac{N_{\text{Av}}}{M_{\text{CO}_2}}, \tag{8}$$

where N_{Av} is Avogadro's number (6.017×10^{23}), $M_{\text{CO}_2} \cong 44.01$ is the molecular weight, and $\sigma_{\text{CO}_2}=14.01\times10^{-24}\ \text{cm}^2$ is total neutron cross section of a CO_2 molecule.

Combining Eqs. (6)–(8), we obtain for the two-phase system (with no adsorption),

$$T_2 = T_1 \exp(-C\rho_{\text{CO}_2}t), \tag{9}$$

where $C \cong 0.19\ \text{cm}^2/\text{g}$ for ρ_{CO_2} in g/cm^3 and a total sample thickness $t=1$ cm (as in our experiments).

Downloaded 21 Dec 2006 to 134.94.122.39. Redistribution subject to AIP license or copyright, see http://jcp.aip.org/jcp/copyright.jsp

In the presence of an adsorbed (third) phase, the transmission will further decrease in comparison to that described by Eq. (9) and the transmission of such a three-phase system is given by

$$T_3 = T_1 \exp - [(N_{\text{unads},CO_2} + N_{\text{ads},CO_2})\sigma_{CO_2} t]. \quad (10)$$

Equation (10) has two unknown parameters: the number density of unadsorbed CO_2 (N_{unads,CO_2}) and the number density of adsorbed CO_2 (N_{ads,CO_2}) which cannot be independently determined from the transmission measurements because both the volume of the adsorbent phase and its density are not known. Following the Gibbs model,[6] we neglect the volume occupied by the adsorbed phase ($V_{\text{ads}}=0$) which is equivalent to the assumption that $N_{\text{unands},CO_2}=N_{CO_2}$. In this case the first term in the right-hand side of Eq. (10) can be approximated by Eq. (8) and the number density of CO_2 molecules in the adsorbed phase should be substituted for the number density of CO_2 corresponding to the excess adsorption (N_e). Thus, Eq. (10) becomes

$$T_3 = T_1 \exp - (N_{CO_2}\sigma_{CO_2} t + N_e \sigma_{CO_2} t)$$
$$= T_2(\exp - N_e \sigma_{CO_2} t), \quad (11)$$

and the value of N_e can be determined through the difference between the transmission of the two-phase and the three-phase systems,

$$N_e = \frac{\ln T_2 - \ln T_3}{\sigma_{CO_2} t}. \quad (12)$$

The excess adsorption n_e can be calculated for an aerogel sample with a known aerogel density ρ_{aerogel},

$$n_e = \frac{M_{CO_2} N_e}{\rho_{\text{aerogel}} N_{\text{Av}}}. \quad (13)$$

C. SANS from multicomponent systems

The coherent cross section $I(Q)$ in units of cm^{-1} of a two-phase system (e.g., a porous silica matrix with homogeneously distributed SC CO_2) is proportional to the neutron contrast between SiO_2 and CO_2 molecules.[13]

$$I(Q) \sim (\rho_1^* - \rho_2^*)^2 = \left(\frac{b_{SiO_2}}{M_{SiO_2}} \rho_{SiO_2} - \frac{b_{CO_2}}{M_{CO_2}} \rho_{CO_2} \right)^2. \quad (14)$$

Here $Q = 4\pi\lambda^{-1} \sin\theta$ where 2θ is the scattering angle, λ is the neutron wavelength, ρ_1^* and ρ_2^* are the scattering length densities of silica and CO_2, respectively, and $b_{SiO_2}=1.58 \times 10^{-12}$ cm and $b_{CO_2}=1.825 \times 10^{-12}$ cm are the scattering lengths of silica and CO_2, respectively. $M_{SiO_2}=60.08$ is the molecular weight and ρ_{SiO_2} is the density of SiO_2. Equation (14) predicts that for a two-phase system (e.g., porous silica matrix with homogeneously distributed CO_2 molecules), the square root of $I(Q)$ should be proportional to the fluid density $I(Q)^{1/2} \sim \rho_{CO_2}$ and thus the formation of a third phase corresponding to the adsorbed fluid will result in deviations from the linear variation of $I(Q)^{1/2}$ versus ρ_{CO_2}. Furthermore, Eq. (14) can be used to calculate the zero average contrast (ZAC) condition at which the neutron contrast between the matrix and the fluid becomes zero and thus $I(Q) \equiv 0$.[14] It may be shown that the ZAC condition can be reached at $\rho_{CO_2} = 1.39$ g/cm^3 if the density of silicon walls of the porous material is taken to be equal to the density of amorphous silica $\rho_{SiO_2}=2.2$ g/cm^3 (which is the case for porous Vycor glass[15]). The skeletal density of silica in aerogel strands is smaller than that of the amorphous silica [$\rho_{SiO_2} \cong 2.0$ g/cm^3 (Ref. 16)] and the calculated ZAC condition in this case corresponds to $\rho_{CO_2}=1.27$ g/cm^3.

The fluid density-dependent invariant $Z_0(\rho_{CO_2})$ for a two-phase system (aerogel homogeneously saturated with CO_2) is given by

$$Z_0(\rho_{CO_2}) = \int_0^\infty Q^2 I_0(Q, \rho_{CO_2}) dQ$$
$$= 2\pi^2 \phi_1 (1 - \phi_1)(\rho_1^* - \rho_2^*)^2, \quad (15)$$

where $I_0(Q, \rho_{CO_2})$ is the coherent cross section in case of zero adsorption and ϕ_1 is the volume fraction of silica in aerogel. If a third (adsorbed) phase is present, the volume fraction can be estimated using a formalism initially developed by Wu[17] to model scattering from microvoids in binary composite materials. For three-phase systems (phase 1=aerogel, phase 2=unadsorbed CO_2, and phase 3=adsorbed CO_2) the scattering invariant is given by[17]

$$Z(\rho_{CO_2}) = \int_0^\infty Q^2 I(Q, \rho_{CO_2}) dQ$$
$$= 2\pi^2 [\phi_1 \phi_2 (\rho_1^* - \rho_2^*)^2 + \phi_2 \phi_3 (\rho_2^* - \rho_3^*)^2$$
$$+ \phi_1 \phi_3 (\rho_1^* - \rho_3^*)^2], \quad (16)$$

where ϕ_i and ρ_i^* are the volume fractions and scattering length densities of the ith phase, respectively. Thus, the volume fraction of the adsorbed phase can be calculated from

$$\phi_3 = \frac{Z - Z_0}{2\pi^2 [\phi_2 (\rho_2^* - \rho_3^*)^2 + \phi_1 (\rho_1^* - \rho_3^*)^2 - \phi_1 (\rho_1^* - \rho_2^*)^2]}. \quad (17)$$

The derivation of Eq. (17) is based on the assumption that the structure of the aerogel matrix does not change when the adsorbed phase is formed. The volume fractions of all three phases should satisfy the following relation:

$$\phi_1 + \phi_2 + \phi_3 = 1. \quad (18)$$

D. Materials

A cylindrical rod of porous Vycor glass 7930 was obtained from Corning Glass Works. The voids in porous Vycor glass are interconnected cylindrical pores with a diameter of 40 Å.[15,18] Base-catalyzed silica aerogels with a nominal density $\rho_{\text{aerogel}}=0.1$ g/cm^3, corresponding to ~96% porosity, were obtained from Oscellus Technologies, Livermore, CA. The aerogels are composed of thin silica strands with the mesh size of 60–70 Å and a highly developed surface area ~700 m^2/g.[16]

The Vycor porous glass and aerogels were shaped into cylinders of 17 mm outside diameter (o.d.), which corre-

Downloaded 21 Dec 2006 to 134.94.122.39. Redistribution subject to AIP license or copyright, see http://jcp.aip.org/jcp/copyright.jsp

sponds to the inside diameter (i.d.) of a SANS stainless steel high-pressure cell fitted with optically polished sapphire windows, which are virtually transparent to neutron radiation. The lengths of the Vycor and aerogel cylinders were chosen to be 6 and 10 mm, respectively, based on the transmission considerations. The optical path of the cell was adjusted to be equal to the length of the aerogel or Vycor glass by inserting sapphire plugs of required thickness. Thus, the internal volume of the cell was completely occupied by the absorber and these experimental conditions correspond to the canonical ensemble versus grand canonical ensemble conditions where the absorber is in a contact with large excess volume occupied by supercritical fluid. The cell was pressurized with CO_2 (Matheson Gas Products, Inc, SFC purity of 99.99%) using a screw-type pressure generator (HIP model 62-6-10). The pressure was measured using a precision digital pressure indicator (Sensotec, model AG-100) and the temperature of the cell was controlled to better than ±0.2 °C using band heaters (Omega). The surface of native (nonoxidized) aerogels is covered by abundant methoxy groups (=Si−O−CH_3) formed during supercritical drying of the precursor gel in supercritical methanol. The alkyl groups can be removed by heating the aerogel to ~500 °C for 2 h, and this process is referred to as "oxidation."[16] Experiments were performed with two aerogel samples, one of them heat untreated (nonoxidized) and the other one heat treated (oxidized). The Vycor glass cylinder was pretreated following the routine described in Ref. 15.

E. SANS and neutron transmission measurements

SANS experiments were performed on the KWS-2 SANS facility at the FRJ2 reactor in Jülich, Germany. The neutron wavelength was $\lambda=6.3$ Å ($\Delta\lambda/\lambda=0.10\%$). Two sample-detector distances (SDDs) of 4 and 1.4 m were used for measuring scattering from the empty aerogel to give an overall range of momentum transfer of $0.01<Q<0.2$ Å^{-1}. The scattering from bulk and confined CO_2 was measured in the appropriate Q range ($0.01<Q<0.07$ Å^{-1}). The transmission at each pressure and temperature was measured continuously *in situ* using He^3 straight beam monitor positioned in the center of the beam stop. The monitor radius was 1 cm which corresponded to solid angles of 2×10^{-5} and 1.6×10^{-4} sr at SDD=4 and 1.4 m, respectively. The solid angle covered by the monitor is small with respect to a solid angle in which most of the SANS signal was observed ($\sim2.8\times10^{-3}$ sr). This minimized level of "contamination" of attenuated neutron intensities by neutrons scattered within the straight beam spot and no systematic deviation in transmission values measured at SDD=4 and 1.4 m at the same pressure and temperature was observed despite more than an order of magnitude larger solid angle "seen" by the monitor at shorter SDD. The SANS data sets were corrected for instrumental backgrounds and normalized to an absolute (±5%) differential cross section per unit sample volume [$I(Q)$ in units of cm^{-1}] by means of precalibrated secondary standards.[19]

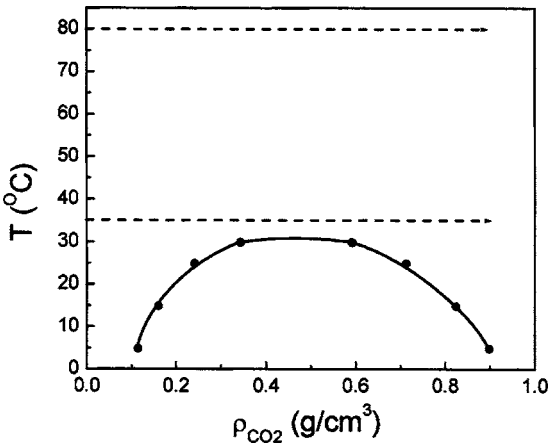

FIG. 1. Coexistence curve of bulk CO_2 calculated using NIST-12 software (Ref. 20). Lines show thermodynamic paths studied in this work.

III. EXPERIMENTAL RESULTS

A. Bulk CO_2

SANS data and transmission values of bulk CO_2 were measured along isotherms $T=35$ °C and $T=80$ °C as a function of pressure in the range of $7.6<P<18$ MPa which is equivalent to the fluid density range of $0.3<\rho_{CO_2}<0.6$ g/cm^3 (see Fig. 1). The fluid density was calculated at each pressure/temperature combination using NIST-12 software.[20] Representative SANS data as a function of density are shown in Fig. 2. The Ornstein-Zernike (OZ) formula

$$I(Q)=\frac{I(0)}{(1+Q^2\xi^2)} \tag{19}$$

was used to extrapolate the cross section at zero angle $I(0)$, which is proportional to the fluid compressibility, and determine the correlation length of the density fluctuations ξ. Data taken at $T=35$ °C, i.e., close to the gas-liquid critical temperature of CO_2 ($T_C=31.1$ °C), reveal maximum in both $I(0,\rho_{CO_2})$ and $\xi(\rho_{CO_2})$ near the critical density of CO_2 $\rho_C=0.468$ g/cm^3 (critical pressure $P_C=7.38$ MPa) where $I_{max}(0,T=35\ °C)\sim1$ cm^{-1} and $\xi_{max}(T=35\ °C)\sim25$ Å. The variation of $I(0)$ and ξ with pressure at $T=80$ °C is more subtle because of the smaller density fluctuations far away

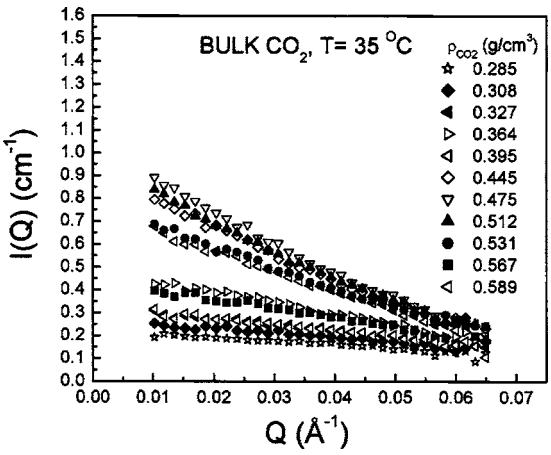

FIG. 2. Density variation of $I(Q)$ from bulk CO_2 at $T=35$ °C.

Downloaded 21 Dec 2006 to 134.94.122.39. Redistribution subject to AIP license or copyright, see http://jcp.aip.org/jcp/copyright.jsp

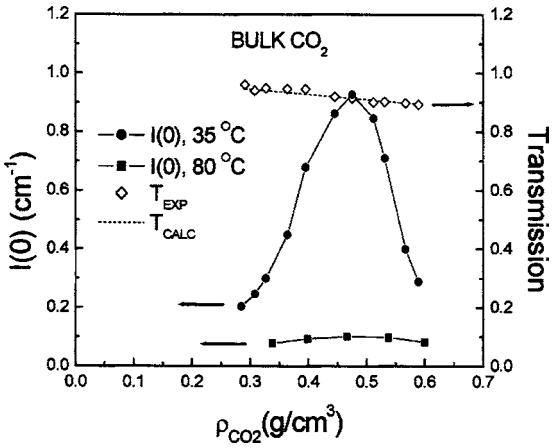

FIG. 3. Density variation of $I(0)$ at two temperatures specified in the inset. Experimental and calculated via Eq. (9) transmissions of bulk CO_2 at different fluid densities (sample thickness of $t=1$ cm) are also shown.

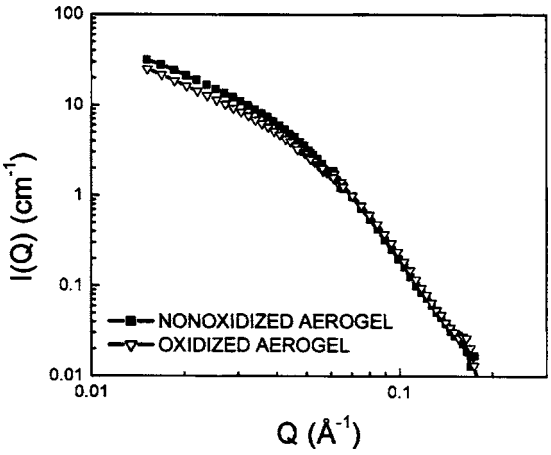

FIG. 5. Neutron cross section of empty aerogels. The lines are fits to Eq. (20).

from the critical point (see Figs. 3 and 4). This behavior is qualitatively similar to that observed in previous x-ray experiments on critical phenomena in CO_2.[21] Figure 3 also demonstrates that experimental transmissions of bulk CO_2 at different pressures agree within experimental error with transmissions calculated via Eq. (9) in which T_1 is set equal to unity (there is no aerogel-related attenuation of neutron beam and thus $T_2 \Rightarrow 1$ as $\rho_{CO_2} \Rightarrow 0$).

B. Blank aerogels

$I(Q)$ obtained from nonoxidized and oxidized aerogels is shown in Fig. 5. We determined that in the intermediate Q range of $0.01 \leqslant Q \leqslant 0.2$ Å^{-1} $I(Q)$ is best described by the following function:[22]

$$I(Q) = \frac{I(0)}{[1+Q^2\xi_G^2]^{(D_f-1)/2}} \frac{\sin[(D_f-1)\tan^{-1}(Q\xi_G)]}{(D_f-1)Q\xi_G}, \quad (20)$$

where ξ_G is the gel correlation length, which represents the large length scale limit of the fractal correlations, and D_f is the fractal dimension. At $Q \sim 0.1$ Å^{-1} a crossover from the Guinier regime ($Q \ll 0.1$ Å^{-1}) to the Porod law behavior is observed. The values of fit parameters are $\xi_G = 87 \pm 8$ Å, $D_f = 1.9 \pm 0.1$ and $\xi_G = 56 \pm 6$ Å, $D_f = 2.2 \pm 0.1$ for nonoxidized and oxidized aerogels, respectively, in agreement with the values of ξ_G and D_f from base-catalyzed aerogels of similar density.[23] Measurements of the "empty" aerogel, with $\rho_{CO_2} = 0$, were repeated after each pressure scan and revealed no changes in either the structural parameters of the aerogel or the transmission after exposure to CO_2.

The effective thickness of silica in aerogels with a density $\rho_{aerogel} = 0.1$ g/cm^3 and density of silica in aerogel strands $\rho_{SiO_2} = 2.0$ g/cm^3 is 0.05 cm. Using the attenuation factor for SiO_2 of $\mu_{SiO_2} = 0.013$ cm^{-1} for $\lambda = 6.3$ Å, we calculate the transmission of the blank aerogel to be $T_1 = 0.9994 \cong 1$, which indicates that the silica in the aerogel strands is virtually transparent to neutrons. However, the measured transmissions of blank nonoxidized and oxidized aerogels ($T_1 = T_0 = 0.749$ and $T_1 = T_0 = 0.796$, respectively) are smaller than unity [see Eq. (6) and Figs. 11 and 12 in Sec. III D]. The relatively low values of T_1 are due to attenuation of the beam by hydrogen nuclei contained in adsorbed moisture and methoxy groups on the aerogel surface.[16] The transmission of oxidized aerogel is higher because of the much lower concentration of alkyl groups, most of which are removed from the surface during high temperature oxidation.

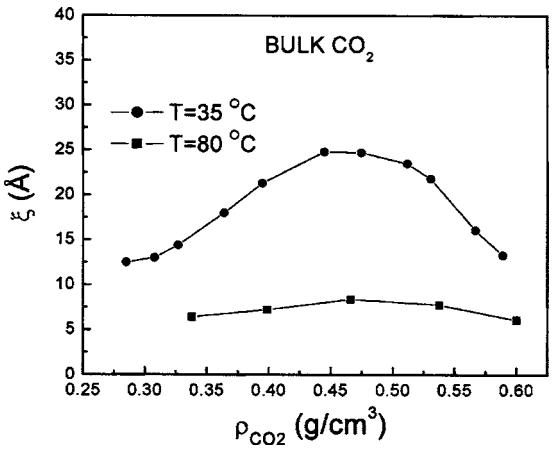

FIG. 4. Density variation of the correlation length at two temperatures specified in the inset.

C. Two-phase system: Porous Vycor glass+SC CO_2

The SANS from Vycor porous glass saturated with SC CO_2 was measured at $T = 35$ °C and $T = 80$ °C as a function of fluid density. The SANS data reveal a characteristic maximum ("correlation" or "Vycor" peak) at $Q_{max} \sim 0.02$ Å^{-1} (Ref. 24) (Fig. 6). The amplitude of the maximum $I(Q_{max})$ was determined and plotted in $I(Q_{max})^{1/2}$ versus ρ_{CO_2} coordinates in Fig. 7, where it may be seen that $I(Q_{max})^{1/2}$ is a linear function of ρ_{CO_2}. A fit to Eq. (14) may be used to calculate the ZAC condition, which is reached at $\rho_{CO_2} = 1.36 \pm 0.06$ g/cm^3. This value corresponds to a scattering length density of 3.39×10^{10} cm^{-2}, in good agreement with $\rho_1^* = 3.35 \times 10^{10}$ cm^{-2}, measured by Wiltzius *et al.*[24] at the Vycor match point. This density also coincides within experimental error with $\rho_{CO_2} = 1.39$ g/cm^3, calculated assuming the

Downloaded 21 Dec 2006 to 134.94.122.39. Redistribution subject to AIP license or copyright, see http://jcp.aip.org/jcp/copyright.jsp

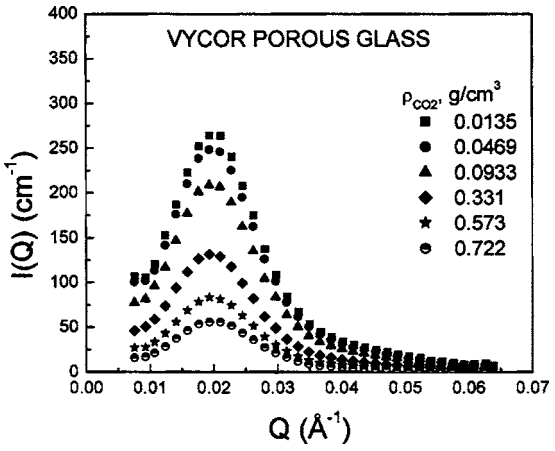

FIG. 6. Neutron cross section of Vycor porous glass saturated with CO_2 at $T=35$ °C. Fluid densities are shown in the inset.

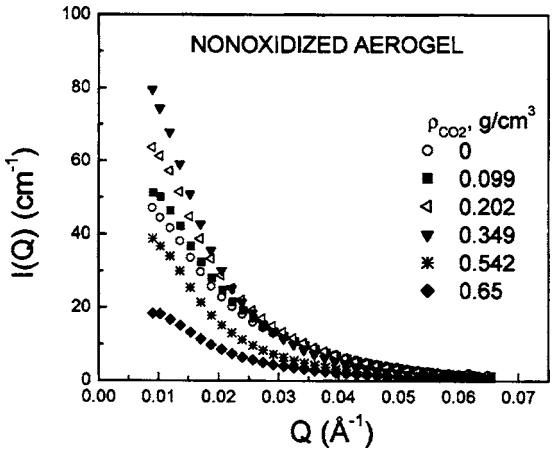

FIG. 8. $I(Q)$ from CO_2 saturated nonoxidized aerogel at $T=35$ °C as a function of density.

density of the solid phase of Vycor glass to be equal to the density of amorphous silica $\rho_{SiO_2}=2.2$ g/cm^3 (see Sec. II C). Thus, the data demonstrate that in the range of temperatures and fluid densities studied, the porous Vycor glass saturated with SC CO_2 represents a two-phase system, with no adsorbed phase present.

D. Three-phase system: Aerogel+SC CO_2

SANS and transmission measurements of oxidized and nonoxidized aerogels saturated with SC CO_2 were performed along two isotherms ($T=35$ and 80 °C) as a function of pressure in the range of $0 \leqslant P \leqslant 25$ MPa, which corresponds to the bulk fluid densities in the range of $0 \leqslant \rho_{CO_2} \leqslant 0.9$ g/cm^3 (see Fig. 1). Unlike for Vycor+SC CO_2 system, the variation of $I(Q)$ versus pressure (or fluid density) for both oxidized and nonoxidized aerogel is nonmonotonic, i.e., the cross section first increases with P and ρ_{CO_2}, reaches a maximum, and decreases at higher density (see Fig. 8). The values of $I(0)$ at different pressures determined using the Guinier formula as well as the variation of $I(0)^{1/2}$ versus ρ_{CO_2} for CO_2 in oxidized and nonoxidized aerogels are shown in Figs. 9 and 10, respectively. A significant *positive* deviation from the straight line corresponding to the two-phase model with $\rho_{SiO_2}=2.0$ g/cm^3 [Eq. (14)] is observed which is quite different from the linear variation of $I(0)^{1/2}$ versus ρ_{CO_2} for SC CO_2 in porous Vycor glass (Fig. 7). The deviation is temperature dependent and is larger at $T \cong T_C$ than at $T \gg T_C$. At $T=35$ °C the maximal values of $I(0)$ exceed those from bulk SC CO_2 by more than two orders of magnitude at the same fluid density, and by more than a factor of 3 of the $I(0)$ from blank aerogels (compare Figs. 2, 5, and 8). The trajectories of curves plotted as $I(0)^{1/2}$ versus

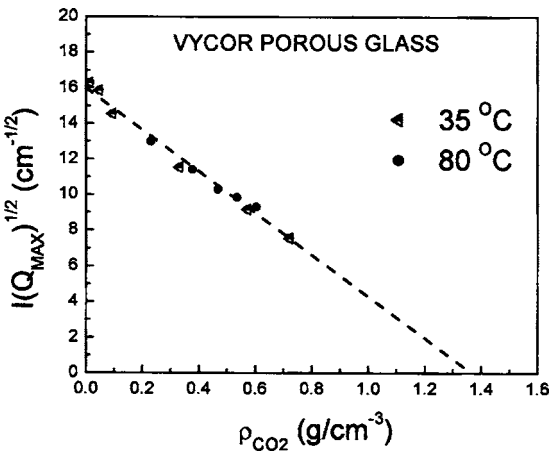

FIG. 7. $I(Q_{max})^{1/2}$ vs density of CO_2 at two different temperatures specified in the inset.

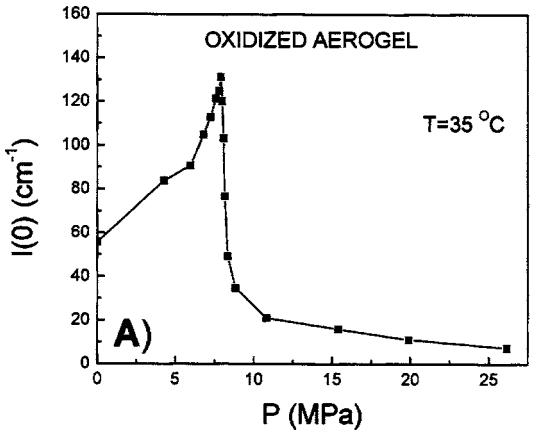

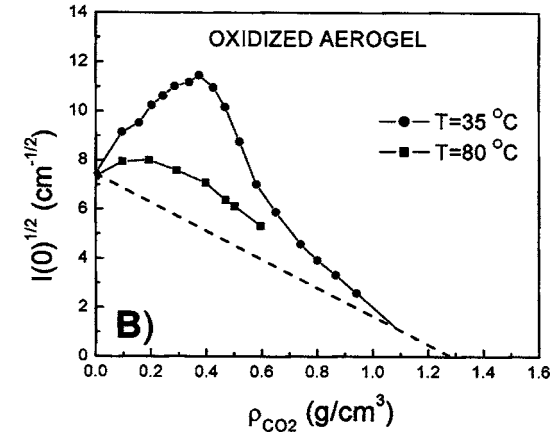

FIG. 9. (A) $I(0)$ as a function of the pressure at $T=35$ °C. (B) $I(0)^{1/2}$ vs ρ_{CO_2} at two temperatures specified in the inset (CO_2 saturated oxidized aerogel).

Downloaded 21 Dec 2006 to 134.94.122.39. Redistribution subject to AIP license or copyright, see http://jcp.aip.org/jcp/copyright.jsp

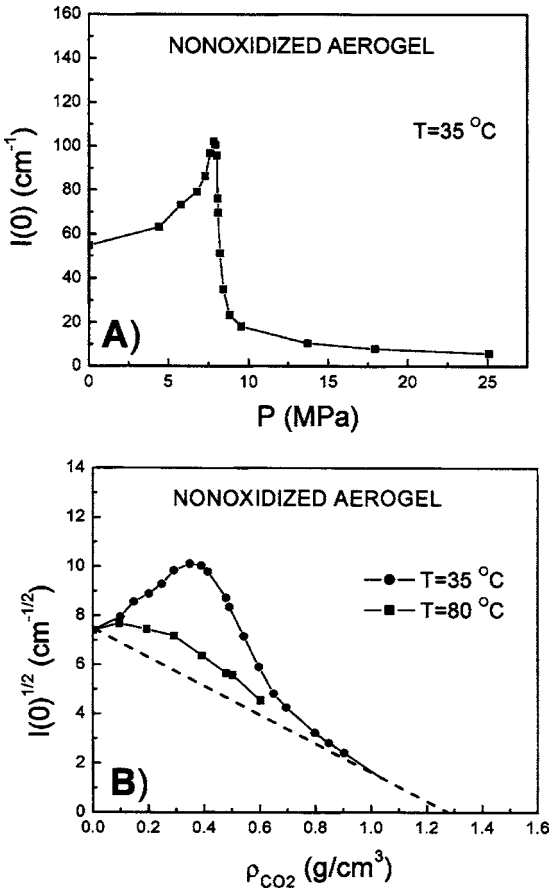

FIG. 10. (A) $I(0)$ as a function of the pressure at $T=35$ °C. (B) $I(0)^{1/2}$ vs ρ_{CO_2} at two temperatures specified in the inset (CO_2 saturated nonoxidized aerogel).

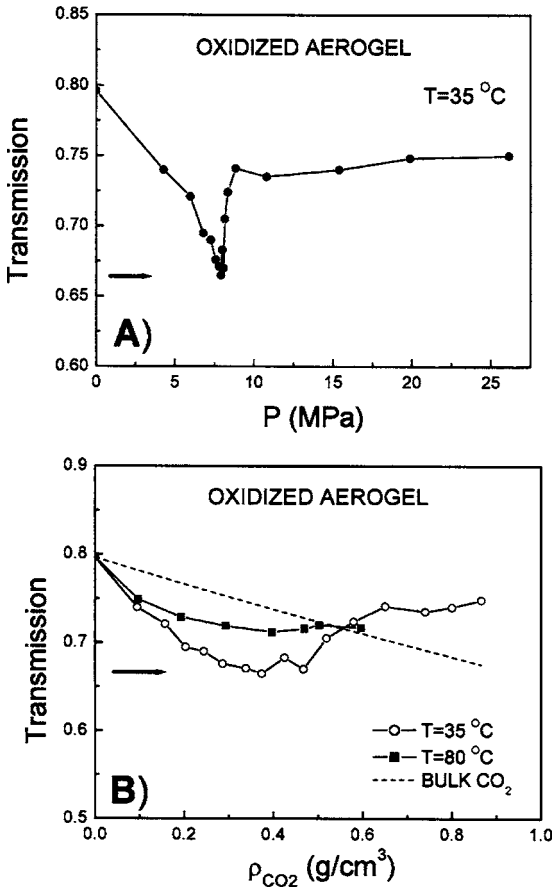

FIG. 11. Transmission of oxidized aerogel vs (A) fluid pressure and (B) density of saturating CO_2 at two temperatures specified in the inset. As is pointed out in the text, the total transmission of blank oxidized aerogel ($T=0.796$) is lower than that of silica in aerogel strands ($T\cong 0.99$) due to additional attenuation of neutron beam by hydrogen nuclei contained in adsorbed moisture and methoxy groups on the aerogel surface. Dashed line is transmission of the imaginary two-phase system (no adsorbed phase) calculated using Eq. (9). Arrows show calculated transmission of the three-phase system at maximal adsorption (see explanations in the text).

ρ_{CO_2} for both oxidized and nonoxidized aerogels tend to cross the straight line at an extrapolated fluid density of $\rho_{CO_2}=1.07\pm0.05$ g/cm^3. We note that the experimental trajectories in Figs. 9(b) and 10(b) converge with the straight lines very slowly. The above error bar corresponds to the accuracy of the linear extrapolation of the three high density points and the actual error bar may be much larger because the real function of $I(0)^{1/2}$ versus ρ_{CO_2} at $\rho_{CO_2}>0.9$ g/cm^3 is not known. The positive deviation from a two-phase model indicates the presence of the third phase (adsorbed CO_2) with an extremely high average scattering length density. The adsorbed CO_2 not only compensates for the decrease of the neutron contrast caused by filling aerogel voids with CO_2 [Eq. (14)], but actually results in the higher contrast between the silica aerogel matrix and the confined fluid, leading to an increase in the scattering cross section. The maximum deviation from a two-phase model is observed at near-critical conditions characteristic of the highest fluid compressibility. It rapidly decreases with pressure due to a suppression of the fluid susceptibility far away from the critical point.

Figures 11 and 12 show the variation of transmission (T) of SC CO_2 saturated oxidized and nonoxidized aerogels as a function of pressure and density. A strong *negative* deviation from the transmission calculated for the two-phase model [Eq. (9)] is observed, both in oxidized and nonoxidized aerogels. The minima of $T(P)$ and $T(\rho_{CO_2})$ at $T=35$ °C correspond to the same pressure and density ($P\cong 7.5$ MPa and $\rho_{CO_2}\cong 0.374$ g/cm^3) at which maxima in $I(0)^{1/2}$ versus ρ_{CO_2} are observed (see Figs. 11 and 12). The transmission of confined SC CO_2 is *lower* than that calculated using Eq. (9) for zero adsorption at the same pressure and temperature, which provides independent confirmation that an adsorbed phase with significantly higher density is present. The minimal values of the transmission are $T_{min}\cong 0.665$ and $T_{min}\cong 0.627$ for oxidized and nonoxidized aerogels, respectively, and at higher fluid densities $\rho_{CO_2}\geqslant 0.6$ g/cm^3 the transmission of both aerogels saturated with SC CO_2 becomes higher than that for the two-phase system. Possible reasons for this behavior are discussed below.

As discussed above, the difference between the transmission of two- and three-phase systems can be used to determine the excess adsorption parameter n_e [Eqs. (12) and (13)], the variation of which as a function of ρ_{CO_2} is shown in Figs. 13. As expected, $n_e(\rho_{CO_2})$ at $T=35$ °C initially increases, goes through a maximum, and then decreases between $0.3<\rho_{CO_2}<0.4$ g/cm^3. Values of n_e for $\rho_{CO_2}>0.4$ g/cm^3 are not shown for reasons discussed below. The excess adsorption is maximal at $\rho_{CO_2}\sim 0.374$ g/cm^3, i.e., at the fluid den-

Downloaded 21 Dec 2006 to 134.94.122.39. Redistribution subject to AIP license or copyright, see http://jcp.aip.org/jcp/copyright.jsp

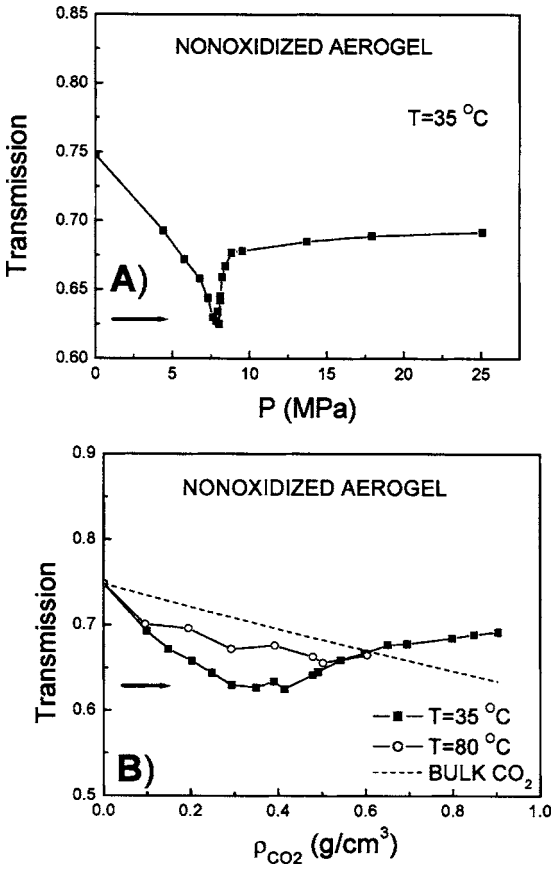

FIG. 12. Transmission of nonoxidized aerogel vs (A) fluid pressure and (B) density of saturating CO_2 at two temperatures specified in the inset. As is pointed out in the text, the total transmission of blank nonoxidized aerogel ($T=0.749$) is lower than that of silica in aerogel strands ($T\cong 0.99$) due to additional attenuation of neutron beam by hydrogen nuclei contained in adsorbed moisture and methoxy groups on the aerogel surface. The transmission of blank nonoxidized aerogel is lower than transmission of blank oxidized aerogel ($T=0.796$) as oxidation removes a fraction of methoxy groups from the aerogel surface at high temperature. Dashed line is transmission of an imaginary two-phase system (zero adsorbed phase) calculated using Eq. (9). Arrows show calculated transmission of the three-phase system at maximal adsorption (see explanations in the text).

sities at which extrema in transmission and $I(0)^{1/2}$ are observed (see Figs. 9–12). The variation of n_e at $T=80\ ^\circ\mathrm{C} \gg T_C$ is much more moderate although qualitatively similar to that near the critical temperature.

The volume fraction of the adsorbed phase (ϕ_3) at different temperatures and pressures can be estimated using the theory of scattering from three-phase systems by Wu[17] [see Eqs. (15)–(17)]. Typical plots of $Q^2I(Q)$ versus Q, based on SANS data from CO_2 saturated oxidized aerogel at different fluid densities, are shown in Fig. 14. The evaluation of the scattering invariant Z corresponding to the area under each curve in Fig. 14 was carried out by the numerical integration in three parts, as the SANS data are only measured between the minimum and maximum Q values, $Q_{\min}$ and $Q_{\max}$. The contribution to the invariant from the (unmeasured) cross section between 0 and $Q_{\min}$ was estimated via the Guinier approximation $[I(Q)\sim\exp(-Q^2R_g^2)]$, extrapolated from the measured cross section at the lowest Q values. Similarly, the contribution to the invariant from the Q range between $Q_{\max}$ and ∞ was estimated via the Porod approximation

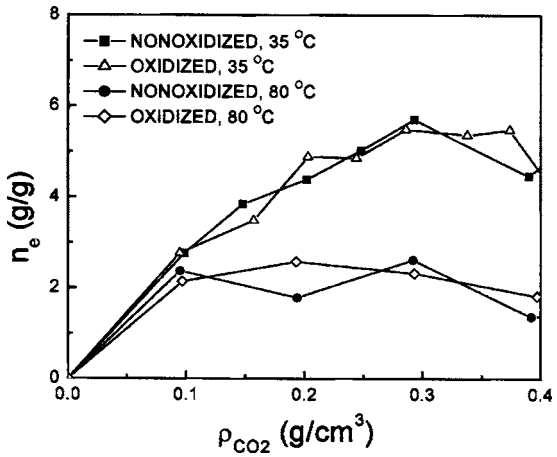

FIG. 13. Excess adsorption of CO_2 in oxidized and nonoxidized aerogels as a function of the fluid density at two temperatures specified in the inset. Data for $\rho_{CO_2}>0.4$ g/cm^3 are not shown for reasons explained in the text.

$[I(Q)\sim Q^{-4}]$, which was used to extrapolate from the measured cross section at the highest Q values.[25] Typically, the low-Q Guinier extrapolation contributed $\sim 1\%$ of the total invariant integral, as this component is weighted by Q^2 in a region where $Q\Rightarrow 0$. The higher-Q (Porod) extrapolation contributed a larger fraction (3%–20%) of the invariant, depending on the pressure, but this approximation generally gave reasonable fits to the data in this region, as expected for systems with sharp interfaces between the phases. A cross-check on the validity of these widely used approximations is that measured invariants are consistent with the calculated invariants for the two-phase model in the limit of $\rho_{CO_2}\Rightarrow 0$ and $\rho_{CO_2}\Rightarrow 1.07$ g/cm^3 (see Fig. 15).

Figure 15 also shows the scattering invariant $Z_0(\rho_{CO_2})$ calculated for a hypothetical two-phase system (CO_2 in aerogel, no adsorption) using Eq. (15) with the following values of parameters: volume fraction of silica in aerogel $\phi_1=0.04$, scattering length density of silica in aerogel strands (assuming physical density of silica $\rho_{SiO_2}=2.0$ g/cm^3) $\rho_1^*=3.16\times 10^{10}$ cm^{-2}, and scattering length density of CO_2 $\rho_2^*=\rho_{CO_2}2.49\times 10^{10}$ cm^{-2}.

According to Wu,[17] the difference between the experimentally measured scattering invariant $Z(\rho_{CO_2})$ and $Z_0(\rho_{CO_2})$

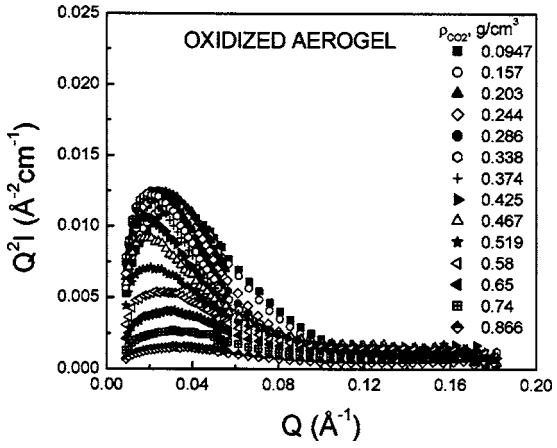

FIG. 14. Typical Kratky plots for CO_2 saturated oxidized aerogel at $T=35\ ^\circ\mathrm{C}$ and different fluid densities specified in the inset.

Downloaded 21 Dec 2006 to 134.94.122.39. Redistribution subject to AIP license or copyright, see http://jcp.aip.org/jcp/copyright.jsp

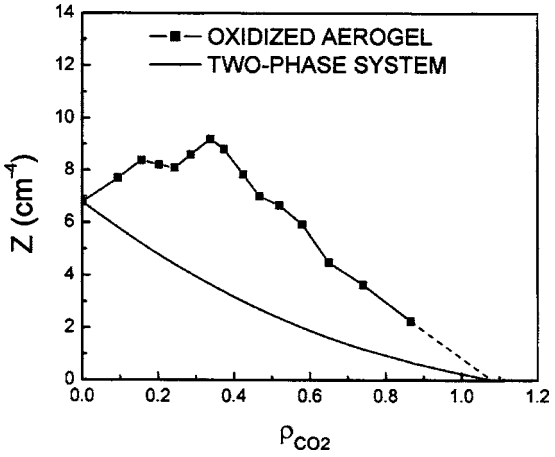

FIG. 15. Scattering invariant of CO_2 saturated oxidized aerogel as a function of the fluid density. Solid line is the scattering invariant of an imaginary two-phase system (zero adsorption) calculated using Eq. (15). Dashed line is extrapolation to $\rho_{CO_2} \sim 1.07$ g/cm^3 at which scattering invariants of the two- and three-phase systems become identical.

is due to the formation of a third phase which in our case corresponds to strongly adsorbed CO_2. The volume fraction of the adsorbed phase ϕ_3 was calculated based on a constant adsorbed-phase-density assumption ($\rho_{ads}=1.07$ g/cm^3) using Eqs. (17) and (18) for the density range up to the maximal adsorption regime at $\rho_{CO_2} \sim 0.374$ g/cm^3 (see Fig. 16). As with measurements of n_e, values of ϕ_3 for $\rho_{CO_2} > 0.4$ g/cm^3 are not shown for reasons explained below.

IV. DISCUSSION AND CONCLUSIONS

SANS has been widely used for characterizing the structure of porous materials as well as investigating the adsorption of liquids in small pores.[14,26–32] This paper describes a new methodology which can be used for studying adsorption of supercritical fluids in porous media by the combination of SANS and neutron transmission techniques. This methodology was applied for the evaluation of the adsorption of SC CO_2 in Vycor porous glass as well as in oxidized and nonoxidized aerogels at constant temperature as a function of pressure.

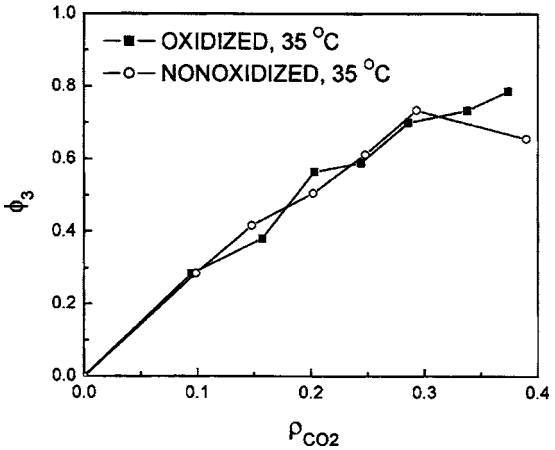

FIG. 16. Variation of the volume fraction ϕ_3 of the adsorbed phase in oxidized and nonoxidized aerogels as a function of ρ_{CO_2}. Calculations are made using Eqs. (17) and (18) under an assumption that the density of adsorbed phase ρ_{ads} is 1.07 g/cm^3 and does not depend on ρ_{CO_2}. Data for $\rho_{CO_2} > 0.4$ g/cm^3 are not shown for reasons explained in the text.

The variation of the adsorption of SC CO_2 in porous materials exhibiting different pore features has been studied by several groups using a variety of experimental methods.[3,4,7,33–40] One of the most common observations is an anomalous peak or "hump" in the adsorption isotherm near the critical point of the bulk fluid. This effect is usually explained as due to the increased compressibility of the fluids in the critical region leading to their high susceptibility to perturbations induced by attractive interactions with the pore surface (critical adsorption). The increased compressibility of the *bulk* CO_2 in the critical region manifests itself as a maximum in $I(0,\rho_{CO_2})$ and $\xi(\rho_{CO_2})$ around the critical fluid density most pronounced at $\rho_{CO_2} \Rightarrow \rho_C$ and $T \Rightarrow T_C$ (see Figs. 3 and 4).[41] The SANS intensity from CO_2 in Vycor porous glass is temperature independent (see Fig. 7), probably because the critical temperature of confined CO_2 is shifted to a much lower value [~ -13 °C (Ref. 40)] and thus density fluctuations in Vycor pores are essentially suppressed at 35 °C, i.e., $\sim 48°$ above the T_C of the confined fluid. Conversely, the SANS from CO_2 in aerogels varies differently at $T=35$ °C $\sim T_C$ and $T=80$ °C $\gg T_C$ because in this case T_C of CO_2 is essentially unaffected by confinement in the aerogel voids.[42] From the point of view of SANS, critical adsorption, which is accompanied by the formation of the dense adsorbed phase, is manifested as a positive deviation of $I(0)^{1/2}$ from the two-phase model [Eq. (14)]. The three-phase model reduces to a two-phase model when the density of the adsorbed phase becomes equal to the density of saturating fluid, which provides an estimate for the density of adsorbed phase: $\rho_{CO_2}=\rho_{ads}=1.07$ g/cm^3 (see Figs. 9 and 10). We note that this value corresponds to the average density of the adsorbed phase with the highest density at the silica surface gradually diminishing with distance towards the pore core. This average density of the adsorbed phase is higher than the saturated liquid density of CO_2 at 7 °C (0.68 g/cm^3) and is similar to the density of close-packed molecules with a diameter corresponding to the van der Waals volume [$\rho_{vdW} \sim 1.03$ g/cm^3 (Refs. 3 and 4)]. This result is consistent with high densities of the adsorbed phase reported by Humauyn and Tomasko for CO_2 adsorbed in activated carbon with the average pore size of 17 Å ($\rho_{ads} \sim 1.03$ g/cm^3) (Ref. 3) as well as in NaY zeolite with the pore sizes in the range of 25 Å ($\rho_{ads} \sim 1.27$ g/cm^3).[4] The formation of an adsorbed CO_2 phase with a density far exceeding that of the bulk fluid ($\rho_{ads} \geqslant 1.1$ g/cm^3) was documented in porous silica with pore diameters in the range of 20–150 Å by Schneider *et al.* using Fourier transform infrared (FTIR).[39] The evidence for the formation of densified CO_2 layers formed in microporous carbon at near-critical conditions was provided by means of neutron powder diffraction (Steriotis *et al.*[36,38]). The significant influence of confinement on liquid-gas phase equilibria of helium, neon, nitrogen and some other fluids was repeatedly demonstrated in experiments by Chan and co-workers,[43–45] Tan and Beamish,[46] and Herman and Beamish.[47–49]

Downloaded 21 Dec 2006 to 134.94.122.39. Redistribution subject to AIP license or copyright, see http://jcp.aip.org/jcp/copyright.jsp

We identify the pressure and density ranges of $0 \leqslant P \leqslant 7.4$ MPa and $0 \leqslant \rho_{CO_2} \leqslant 0.4$ g/cm^3 as a strong adsorption regime in which the pressurizing of aerogels with CO_2 leads to formation of the adsorbed phase until the majority of small aerogel pores with sizes 60–70 Å are filled. This behavior is accompanied by an increased deviation from the two-phase model as documented in variations of both $I(0,\rho_{ads})$ and the transmission $T(\rho_{ads})$ (see Figs. 9–12). It is usually assumed in the literature that after maximum adsorption is reached, the density of the adsorbed phase does not change significantly with pressure[3,4] and thus ρ_{ads} corresponding to the maximal adsorption can be set equal to $\rho_{ads}=1.07$ g/cm^3 which is supported by the following considerations. The data shown in Fig. 16 demonstrate that 78% of the void volume in the maximal adsorption regime is filled with the adsorbed phase and thus ~18% of V_{void} is accessible to unadsorbed SC CO_2. Using Eq. (9) with $\rho_{CO_2}=(0.78\times 1.07+0.18\times 0.347)$ g/cm^3 we calculate the transmission of the aerogel $T=0.670$ which correlates well with the measured value of $T=0.665$ (see Fig. 11). Similarly, the calculated transmission agrees with the experimental result for the nonoxidized aerogel (see Fig. 12).

The variation of transmission at $\rho_{CO_2} > 0.4$ g/cm^3 is somewhat puzzling. As observed in Figs. 11 and 12, in this range of fluid densities the $T(\rho_{CO_2})$ of CO_2 saturated aerogels starts to increase and finally exceeds the transmission of a two-phase system at $\rho_{CO_2} \geqslant 0.6$ g/cm^3. This effect is reproduced for both nonoxidized and oxidized aerogels, but was not observed for propane-saturated aerogels where the transmission always remained lower than that of the two-phase system with zero adsorption.[50] The physical origin of such behavior is not completely clear and we tentatively ascribe it to the depletion of the (highly developed) surface of aerogel strands with CO_2 molecules at elevated pressures. If this assumption is valid, the initially three-phase system can develop a fourth phase at elevated densities ($\rho_{CO_2} \geqslant 0.4$ g/cm^3). In this regime, the values of n_e and ϕ_3 calculated based on the three-phase model may be incorrect, and because the variation of the volume of the depleted near-surface layer with ρ_{CO_2} is not known, we are not able to calculate the transmission to a better approximation. Thus, the values of n_e in Fig. 13 and ϕ_3 in Fig. 16 are presented only in the strong adsorption regime where the depletion effect is zero or negligibly small.

Analysis of the available literature on adsorption of SC CO_2 (Ref. 3, 4, 7, and 33–39) demonstrates that the maximal values of the excess adsorption in the near-critical conditions vary generally in the range between 5 mmol/g (zeolites) and 20 mmol/g (superactivated carbon) which translates into $0.2 \leqslant n_e(\mathrm{g/g}) \leqslant 0.9$. It follows, then, from the data shown in Fig. 13, that the maximal excess adsorption of SC CO_2 in aerogels at $T=35$ °C ($n_e \sim 5.74$ g/g) far exceeds n_e for CO_2 in different adsorbers, and this is related to extremely high porosity (large values of V_{void}) and optimum pore sizes of aerogels investigated in this study. Using $\rho_{ads}=1.07$ g/cm^3 and $n_e=5.74$ g/g for a CO_2 saturated oxidized aerogel in the maximal adsorption regime we calculate from Eq. (5) the corresponding value of absolute adsorption $n^{abs}=8.8$ g/g. An independent cross-check of this value can be performed as follows. Using the value of $V_{aerogel}=V_{cell}=2.27$ cm^3 and $\rho_{ads}=1.07$ g/cm^3, we calculate the mass of adsorbed CO_2 $m_{CO_2}=1.94$ g. The mass of silica in the aerogel cylinder with density $\rho_{aerogel}=0.1$ g/cm^3 is $m_{aerogel}=2.27\times 0.1=0.227$ g. Thus, the absolute adsorption value corresponding to the maximal adsorption regime is $n^{abs}=m_{CO_2}/m_{aerogel} \cong 8.5$ g/g which agrees well with the value $n_{abs}=8.8$ g/g obtained based on the SANS data and transmission measurements.

In conclusion, SANS and neutron transmission techniques were applied for the first time to characterize the adsorption of SC CO_2 in nonoxidized and oxidized aerogels as a function of pressure. The results demonstrate the formation of a highly densified adsorbed phase with a density ~1.07 g/cm^3 ($T=35$ °C), which is close to the density corresponding to close-packed CO_2 molecules with the van der Waals volume. The excess adsorption of CO_2 is found to be virtually independent of oxidation, though it depends strongly on the proximity to the critical point of the bulk fluid. CO_2 molecules do not adsorb on the pore walls of Vycor porous glass due to significant suppression of the critical temperature of the confined fluid. In CO_2-saturated aerogels, the maximal adsorption is reached at the bulk fluid density $\rho_{CO_2} \sim 0.374$ g/cm^3. The volume fraction of the adsorbed phase here reaches ~78% and the values of the excess and absolute adsorptions are $n_e=5.74$ and $n_{abs}=8.8$ g/g, respectively. Such a high capability of aerogels to absorb significant amounts of SC CO_2, as compared with other adsorbents, may be of interest in CO_2 separation and storage technology applications. The methodology described in this paper can be used for studies of high-pressure adsorption of various individual supercritical fluids in different adsorbents of practical importance. It can also be extended to adsorption studies of supercritical fluid *mixtures* in porous materials using deuterium labeling methods on one of the components.[42] One of the interesting applications of the described methodology might be the investigation of the adsorption of carbon dioxide, methane, and their mixtures in various coals at different temperatures and pressures. The results of such studies could be important for the sequestration of CO_2 in deep coal seams as well as for the methane drainage industry.[51,52]

ACKNOWLEDGMENTS

We gratefully acknowledge P. E. Wolf for careful reading the manuscript, stimulating discussions, and sharing with us the data on confined ^{4}He prior to publication. This research was sponsored by the Laboratory Directed Research and Development Program and by the Divisions of Materials Sciences and Engineering and Chemical Sciences, Geosciences, and Biosciences, Office of Basic Energy Sciences, U.S. Department of Energy under Contract No. DE-AC05-00OR22725, Oak Ridge National Laboratory, managed by UT-Battelle, LLC.

[1] *Supercritical Fluids: Fundamentals for Applications*, edited by E. Kiran and J. M. H. Levelt-Sengers (Kluwer Academic, Dodrecht, 1993).
[2] A. Baiker, Chem. Rev. (Washington, D.C.) **99**, 453 (1999).
[3] R. Humauyn and D. L. Tomasko, AIChE J. **46**, 2065 (2000).

Downloaded 21 Dec 2006 to 134.94.122.39. Redistribution subject to AIP license or copyright, see http://jcp.aip.org/jcp/copyright.jsp

[4] W. Gao, D. Butler, and D. L. Tomasko, Langmuir **20**, 8083 (2004).
[5] S. Blumel and G. H. Findenegg, Phys. Rev. Lett. **54**, 447 (1985).
[6] S. Sircar, Ind. Eng. Chem. Res. **38**, 3670 (1999).
[7] M. Sudibandriyo, Z. Pan, J. E. Fitzgerald, R. L. Robinson, Jr., and K. A. M. Gasem, Langmuir **19**, 5323 (2003).
[8] R. Staudt, G. Saller, M. Tomalla, and M. Keller, Ber. Bunsenges. Phys. Chem. **97**, 98 (1993).
[9] T. Hocker, A. Rajendran, and M. Mazzotti, Langmuir **19**, 1254 (2003).
[10] C. Zhou, F. Hall, K. A. Gasem, and R. L. Robinson, Jr., Ind. Eng. Chem. Res. **33**, 1280 (1994).
[11] P. Strunz, J. Saroun, U. Keiderling, A. Wiedenmann, and R. Przenioslo, J. Appl. Crystallogr. **33**, 829 (2000).
[12] D. A. Bostain, J. S. Brenizer, Jr., and P. M. Norris, Res. Nondestruct. Eval. **14**, 47 (2002).
[13] G. D. Wignall and Y. B. Melnichenko, Rep. Prog. Phys. **68**, 1761 (2005).
[14] C. I. Merzbacher, J. G. Baker, K. E. Swider, J. V. Ryan, R. A. Bernstein, and D. R. Rolison, J. Non-Cryst. Solids **255**, 234 (1998).
[15] M. Agamalian, J. M. Drake, S. K. Sinha, and J. D. Axe, Phys. Rev. E **55**, 3021 (1997).
[16] K. Tajiri, K. Igarashi, and T. Nishio, J. Non-Cryst. Solids **186**, 83 (1995).
[17] W. L. Wu, Polymer **23**, 1907 (1982).
[18] Vycor brand porous thirsty glass No. 7930, Corning Technological Brochure, Corning Glass Works, OEM Sale Service, Box 5000, Corning, NY 14830.
[19] G. D. Wignall and F. S. Bates, J. Appl. Crystallogr. **20**, 28 (1987).
[20] http://www.nist.gov/srd/nist12.htm
[21] B. Chu and J. S. Lin, J. Chem. Phys. **53**, 4454 (1970).
[22] T. Freltoft, J. K. Kjems, and S. K. Sinha, Phys. Rev. B **33**, 269 (1986).
[23] R. Vacher, T. Woignier, J. Pelous, and E. Courtens, Phys. Rev. B **37**, 6500 (1988).
[24] P. Wiltzius, F. S. Bates, S. B. Dierker, and G. D. Wignall, Phys. Rev. A **36**, 2991 (1987).
[25] J. S. Lin, R. W. Hendricks, L. A. Harris, and C. W. Yust, J. Appl. Crystallogr. **11**, 621 (1978).
[26] M. J. Benham, J. C. Cook, J.-C. Li, D. K. Ross, P. L. Hall, and B. Sarkissian, Phys. Rev. B **39**, 633 (1989).
[27] J. C. Li, D. K. Ross, and M. J. Benham, J. Appl. Crystallogr. **24**, 794 (1991).
[28] J. C. Li, D. K. Ross, L. D. Howe, K. L. Stefanopoulos, J. P. A. Fairclough, R. Heenan, and K. Ibel, Phys. Rev. B **49**, 5911 (1994).
[29] C. I. Merzbacher, J. G. Baker, K. E. Swider, and D. R. Rolison, J. Non-Cryst. Solids **224**, 92 (1998).
[30] W. L. Wu, W. E. Wallace, E. K. Lin, G. W. Lynn, C. J. Glinka, E. T. Ryan, and H. M. Ho, J. Appl. Phys. **87**, 1193 (2000).
[31] J. D. F. Ramsay and S. Kallus, J. Non-Cryst. Solids **285**, 142 (2001).
[32] R. C. Hedden, H. J. Lee, C. L. Soles, and B. J. Bauer, Langmuir **20**, 6658 (2004).
[33] J. R. Strubinger, H. Song, and J. F. Parcher, Anal. Chem. **63**, 98 (1991).
[34] J. H. Chen, D. S. H. Wong, C. S. Tan, R. Subramanian, C. T. Lira, and M. Orth, Ind. Eng. Chem. Res. **36**, 2808 (1997).
[35] O. Di Giovanni, W. Dorfer, M. Mazzotti, and M. Morbidelli, Langmuir **17**, 4316 (2001).
[36] T. A. Steriotis, K. L. Stefanopoulos, A. C. Mitropoulos, N. K. Kanellopoulos, A. Hoser, and M. Hofmann, Appl. Phys. A: Mater. Sci. Process. **74**, S1333 (2002).
[37] L. Zhou, S. Bai, W. Su, J. Yang, and Y. Zhou, Langmuir **19**, 2683 (2003).
[38] T. A. Steriotis, K. L. Stefanopoulos, N. K. Kanellopoulos, A. C. Mitropoulos, and A. Hoser, Colloids Surf., A **241**, 239 (2004).
[39] M. S. Schneider, J. D. Grunwaldt, and A. Baiker, Langmuir **20**, 2890 (2004).
[40] C. G. V. Burgess, D. H. Everett, and S. Nuttall, Pure Appl. Chem. **61**, 1845 (1989).
[41] Qualitatively similar behavior demonstrated He^4 confined in aerogel of a similar density [P. E. Wolf (private communication)].
[42] Y. B. Melnichenko, G. D. Wignall, D. R. Cole, and H. Frielinghaus, Phys. Rev. E **69**, 057102 (2004).
[43] A. P. Y. Wong and M. H. W. Chan, Phys. Rev. Lett. **65**, 2567 (1990).
[44] A. P. Y. Wong, S. B. Kim, W. I. Goldburg, and M. H. W. Chan, Phys. Rev. Lett. **70**, 954 (1993).
[45] R. Garcia, S. Scheidemantel, K. Knorr, and M. H. W. Chan, Phys. Rev. E **68**, 056111 (2003).
[46] H. W. Tan and J. R. Beamish, Physica B **284–288**, 389 (2000).
[47] T. Herman and J. R. Beamish, J. Low Temp. Phys. **126**, 661 (2002).
[48] T. Herman and J. R. Beamish, J. Low Temp. Phys. **141**, 193 (2005).
[49] T. Herman and J. R. Beamish, Phys. Rev. B **72**, 184202 (2005).
[50] Y. B. Melnichenko, G. D. Wignall, and D. R. Cole (unpublished).
[51] J. W. Larsen, Int. J. Coal Geol. **57**, 63 (2004).
[52] K. Gatnar and A. Tor, Appl. Energy **74**, 331 (2003).

Downloaded 21 Dec 2006 to 134.94.122.39. Redistribution subject to AIP license or copyright, see http://jcp.aip.org/jcp/copyright.jsp